DEVELOPMENTAL DYNAMICS 247:1018–1027, 2018
DOI: 10.1002/DVDY.24637

Novel Approaches to Study Coronary Vasculature Development in Mice

Hana Kolesová [1,2]* Martin Bartoš,[1,3] Wan Chin Hsieh,[1] Veronika Olejníčková,[1,2] and David Sedmera [1,2]

[1]Institute of Anatomy, First Faculty of Medicine, Charles University in Prague, Czech Republic
[2]Institute of Physiology, Czech Academy of Sciences, Prague, Czech Republic
[3]Institute of Dental Medicine, First Faculty of Medicine, Charles University in Prague, Czech Republic

Background: Coronary artery development is an intensely studied field. Mice are a popular genetic model for developmental studies, but there is no widely accepted protocol for high-throughput, high-resolution imaging of their developmental and adult coronary artery anatomy. Results: Using tissue-clearing protocols and confocal microscopy, we have analyzed embryonic and juvenile mouse hearts in *Cx40:GFP* knock-in models with a special focus on septal artery development. We found that the septal artery, which supplies the interventricular septum, was initially formed as an arterial plexus that connected to both the left and right coronary arteries. During development, the plexus was remodeled into a single tube, which then remained connected only to the right coronary artery. Since optical imaging became limited at postnatal stages, it was supplemented with injection techniques using India ink and Microfil; the latter was subsequently analyzed with micro-CT to visualize the anatomy of coronary vessels in 3D. Conclusions: The techniques described here enable us to study the finer details of coronary artery development in mice and can, therefore, be implemented to study the pathogenesis of coronary malformations in various mouse models. *Developmental Dynamics 247:1018–1027, 2018*. © 2018 Wiley Periodicals, Inc.

Key words: Coronary artery anatomy; coronary anomalies; GFP; connexin40; embryonic development; heart

Submitted 16 January 2018; First Decision 4 May 2018; Accepted 8 May 2018; Published online 17 May 2018

Introduction

Mice are used extensively to study cardiovascular embryology and pathophysiology, with the aim to determine the molecular basis of coronary artery development and congenital heart disease (Andersen et al., 2014), and to study atherosclerosis (Lee et al., 2017). Accurate knowledge of coronary artery anatomy is, therefore, of paramount importance for experimental and clinical studies using the murine model. For instance, experimental coronary occlusion (to simulate myocardial infarction) usually involves ligating the proximal segment of the left coronary trunk (Michael et al., 1995); hence, variability in the origin, level, or proportion of animals with a septal artery originating from the left coronary trunk could have a significant impact on the infarct area and experimental results. Furthermore, the available data on murine coronary anatomy suggests that common strains of laboratory mice can harbor coronary artery patterns that are similar to human congenital anomalies that can cause sudden death; hence, they may be utilized as animal models of important, life-threatening human diseases (López-García et al., 2016).

The three main coronary arteries in mice—the right coronary artery (RCA), the left coronary artery (LCA), and the septal artery—are intramyocardial, as in other rodents (Durán et al., 1992; Fernandez et al., 2008). The RCA arises from the right aortic sinus and crosses the dorsal wall of the right ventricle obliquely before turning toward the apex as the dorsal interventricular artery; the LCA arises from the left aortic sinus and divides into the left circumflex artery and the obtuse marginal artery before extending to the apex; the septal artery originates either from the main RCA trunk or independently from the right aortic sinus to supply the interventricular septum (Durán et al., 1992; Icardo and Colvee, 2001; Clauss et al., 2006). However, in spite of this general appreciation of murine coronary anatomy, relatively few detailed studies of coronary artery anatomy or variability have been undertaken. The limited data that does exist suggest that unusual coronary artery arrangements such as high takeoff, double origins, a single coronary orifice, and slit-like openings occur with significant frequency in mice and are similar to some coronary anomalies that are found in humans (Icardo and Colvee, 2001). However, these studies used techniques such as gross macroscopic examination or vascular corrosion casting (Durán et al., 1992; López-García et al., 2016), both of which

Additional supporting information may be found online in the Supporting Information section at the end of the article.
Grant sponsor: Grant Agency of the Czech Republic, Ministry of Education, Youth and Sports of the Czech Republic; Grant number: 13-12412S; Grant sponsor: Czech Academy of Sciences; Grant number: 67985823; Grant sponsor: Charles University UNCE; Grant numbers: 204013, SVV.
*Correspondence to: Hana Kolesová, Institute of Anatomy, First Faculty of Medicine, Charles University, U Nemocnice 3, 12800 Prague, Czech Republic. E-mail: hana.kolesova@lf1.cuni.cz

Article is online at: http://onlinelibrary.wiley.com/doi/10.1002/dvdy.24637/abstract

miss the detail, are difficult to perform, or lack the resolution to map very small vessels.

Connexin40 (Cx40) is a conserved cardiac gap junction protein that, in addition to its well characterized expression in atrial myocytes and parts of the conduction system, is also expressed in arterial endothelial cells (Miquerol et al., 2004; Benes et al., 2014). Therefore, transgenic mice in which the enhanced green fluorescent protein (GFP) marker is expressed, instead of the *Cx40* gene, show coronary artery–specific GFP expression. Homozygous Cx40:GFP knock-in mice were first described in 2004 (Miquerol et al., 2004) and are functionally null mice that remain viable and fertile. This is a result of the knock-in, which disrupts the endogenous Cx40 gene expression. Mice homozygous for the Cx40 deletion present with hypertension (Wagner et al., 2007) and an increased incidence of congenital heart disease (Simon et al., 1998). In addition, there is a conduction phenotype that includes a right bundle branch block (van Rijen et al., 2001) and abnormal atrial conduction (Leaf et al., 2008; Benes et al., 2014). However, heterozygotes have normal hearts with GFP expression mimicking that of the endogenous *Cx40* gene (Sankova et al., 2012). This model provides the opportunity to perform detailed whole-mount coronary artery anatomy studies using confocal microscopy and high-resolution imaging with 3D reconstructions, without sectioning the heart tissue. On the condition that the fluorescence is preserved during tissue processing, this model enables visualization of the vessels at a greater depth (Kolesová et al., 2016).

Here we combine the *Cx40:GFP* knock-in mouse model with tissue-clearing protocols to optimally visualize and map the coronary artery anatomy in prenatal (embryonic day [ED] 16.5 and 18.5) and juvenile mouse hearts in whole-mount by confocal microscopy. This approach is compared to coronary artery injection methods in juvenile hearts, with either India ink or radiopaque Microfil polymer; the latter can be analyzed in 3D with a micro computed tomography (micro-CT) scanner. We focus particularly on characterization of the septal artery formation to validate the utility of this novel coronary artery imaging approach.

Results

Prenatal Development of Coronary Arteries

Using a confocal microscope, embryonic hearts of heterozygous *Cx40:GFP* knock-in mice at ED16.5 (Fig. 1) and ED18.5 (Fig. 2) were analyzed as whole-mounts cleared with CUBIC or SCALE. At ED16.5, the coronary arteries were already well established and the arterial endothelium was positive for GFP throughout its length. The LCA and RCA were clearly visible in their entire length as they originated from the aorta to vascularize the left and right ventricles, respectively (Fig. 1A,B). Although there was significant GFP expression in the ventricular trabeculae, the developing coronary vasculature was clearly distinguishable, as it was limited to the superficial layers of the heart (Fig. 1C,D). It was possible to follow not only the main trunks, but also the small developing branches, for example, of the RCA (Fig. 1C,D). The main trunks of the RCA and LCA were completely developed at their proximal parts; however, their distal apical parts were still forming from the arterial plexuses and single endothelial cells, which were also visible as they were positive for GFP (Fig 1. A,B). At this stage, the septal artery was connected through the vascular plexus to both coronary arteries.

Two days later, at ED18.5, the development of the coronary arteries was more advanced. Coronary vasculature was fully developed and branches had formed up to the apical part of the heart (Fig. 2A,B), as observed in the newborn mice. All parts of the coronary arteries were positive for GFP, i.e., the main trunks, and their branches leading up to the terminal small arterioles (Fig. 2). The RCA had four main branches descending along the right aspect of the heart to supply the right ventricle: The conus artery (*ramus coni arteriosi*) and proximal branch of the right ventricle (*ramus proximalis ventriculi dextri*) arose from the top right aspect of the RCA, respectively, followed by the marginal branch (*ramus marginis ventriculi dextri*) and, last, the distal branch (*ramus distalis ventriculi dextri*) (Figs. (1 and 2)B). In the LCA, the following branches were already formed: the left circumflex artery (*ramus circumflexus sinister*) and its three branches—the proximal branch of the left atrium (*ramus proximalis atrii sinistri)*, the intermediate branch of the left atrium (*ramus intermedius atrii sinistri*), and the distal branch of the left atrium (*ramus distalis atrii sinistri*). Subsequently, the LCA gave off three main branches posteriorly: the proximal branch (*ramus proximalis ventriculi sinistri)*, followed by the left proximal collateral branch (*ramus collateralis sinister proximalis*) and the left distal collateral branch (*ramus collateralis sinister distalis*). Anterior branches of the LCA were smaller and named as the branches of the ventricle (*rami ventriculares*) (Fig. 2A,B).

The endothelial lining of the outflow tract was GFP-positive in both the embryonic stages studied. In all embryonic and juvenile specimens analyzed, GFP positivity was not observed in the endothelial lining of veins or in any other layers of the arteries.

Development of the septal artery

In mice, the interventricular septum is supplied by the septal artery. In our study, the formation of the septal artery was monitored during embryonic development. At ED16.5, the septal artery was originating from an arterial plexus located between the RCA and LCA. This developing plexus was connected to both main trunks of the LCA and RCA in this stage (Fig. 3A,B). In some embryos at ED16.5, the future development was already distinguishable, and the connection to the RCA was thicker than that of the LCA (Fig. 3B). The arterial plexus then gradually remodeled into a single trunk to form the septal artery, after which it lost its connections to the LCA via small arterioles. Finally, at ED18.5, there was only one trunk of the septal artery present that was connected exclusively to the RCA. In all 23 embryos analyzed, the septal artery remained connected only to the RCA, as observed in adult mice; we have not found a single case where the septal artery was a branch of the LCA (Fig. 3C).

Postnatal Coronary Artery Imaging

Juvenile Cx40:GFP mice

We analyzed the coronary arteries in juvenile and adult mice in the *Cx40:GFP* model in a manner similar to the way the embryos were analyzed. In juvenile and adult mice, GFP positivity was present in all coronary artery branches, as it was in the embryos. We were able to detect a positive endothelial lining in the main branches of the RCA and the LCA (Fig. 4). However, whole-heart confocal imaging and analysis, which worked well on smaller embryonic hearts, was not feasible on the juvenile and adult hearts. The main obstacles to this method were the size of the

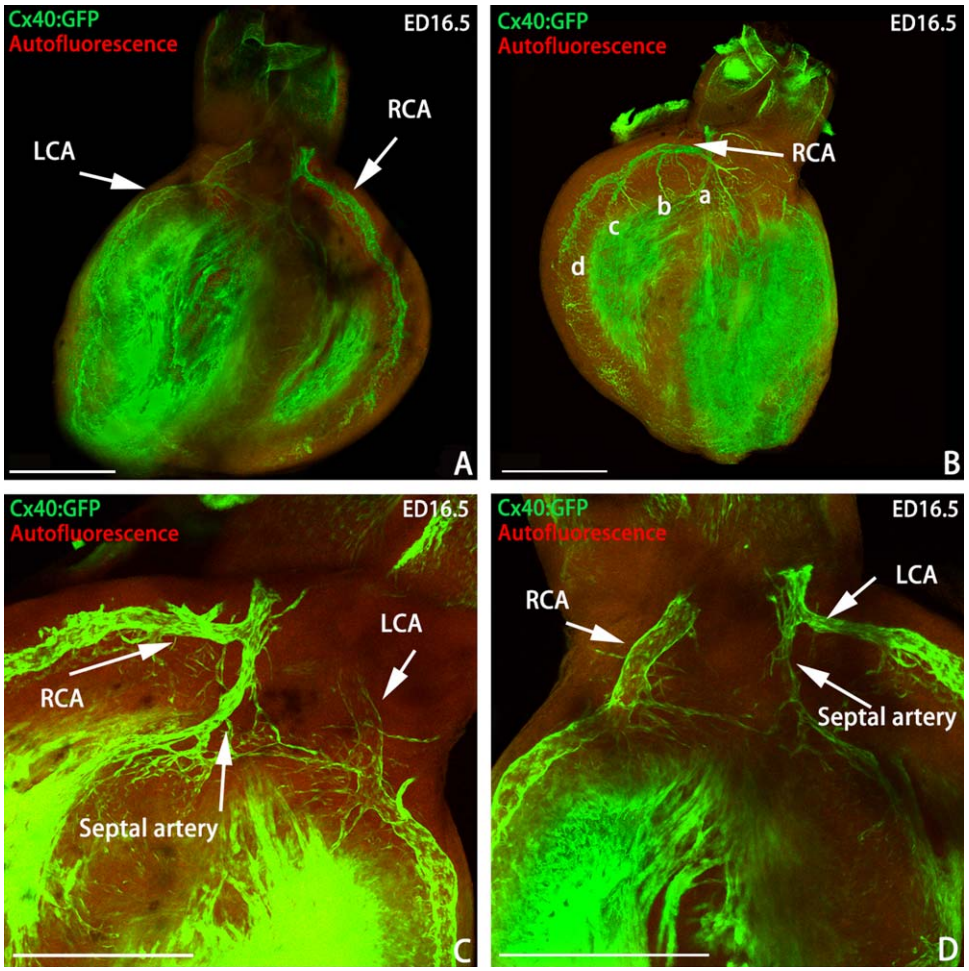

Fig. 1. Coronary arteries at ED16.5 in *Cx40:GFP* transgenic mouse in whole-mount confocal microscopy. Cx40 expression in coronary arteries and trabeculae is in green and tissue autofluorescence is in red. **A**: Overview of developing left (LCA) and right (RCA) coronary arteries in the whole heart. The proximal parts of the coronary arteries are formed, while the distal parts are still developing. Z-stack from 18 sections, 25 μm per section. **B**: Developing right coronary artery and its branches: a, conus artery (*ramus coni arteriosi*); b, proximal branch of the right ventricle (*proximalis ventriculi dextri*); c, marginal branches of the right ventricle (*ramus marginis ventriculi dextri*); d, distal branches of the right ventricle (*ramus distalis ventriculi dextri*). Z-stack from 21 sections, 25 μm per section. **C,D**: Details of the LCA and RCA origins. Note the developing septal artery and small arterioles in the region, which are also positive for Cx40. Z-stacks from 18 and 16 sections, respectively, 15 μm per section. Scale bars = 200 μm.

hearts and the significant autofluorescence of the myocardium, which rendered creation of large 3D stacks from optical sections challenging. Even though the endothelial lining of the arteries was distinguishable from the background in a single optical section, the Z-stack was relevant only if an artery was parallel to the imaging plane (XY); however, the deeper signal was obscured by a strongly autofluorescent myocardium (Fig. 4). The septal artery was present as a single tube branching from the RCA, and no trace of the endothelial network or of its former connection via the plexus to the LCA was found (Fig. 4A,B).

India ink injection

As a classical method of visualizing the coronary vasculature, a retrograde injection via the ascending aorta was used. With light microscopy imaging, we were able to visualize the main superficial branches of the coronary vasculature, such as the anterior ventricular arteries of the RCA, the circumflex artery, etc. (Fig. 5). The coronary arteries were not completely filled with the injecting medium, as the particles of India ink varied in size and shape, thereby also limiting its injection into smaller arterioles. India ink injection proved to be a fast and relatively cheap method, which permitted visualization of the general structure of the coronary vasculature in whole-mount juvenile and adult hearts (Fig. 5).

Microfil injection and micro-CT analysis

The third visualization method used to test for coronary arteries was their retrograde injection with Microfil, a low-viscosity three-component polymer that polymerizes in the vascular system. In majority of our juvenile injected hearts, Microfil passed through the capillaries to the venous network and allowed visualization of the main venous stems (Fig. 6B,D). Capillaries could not be viewed, as their injection required special viscosity (according to the manufacturer) and our main goal was to visualize the arteries. As this method is based upon injection, it visualized only the vessels, which could be reached by the medium.

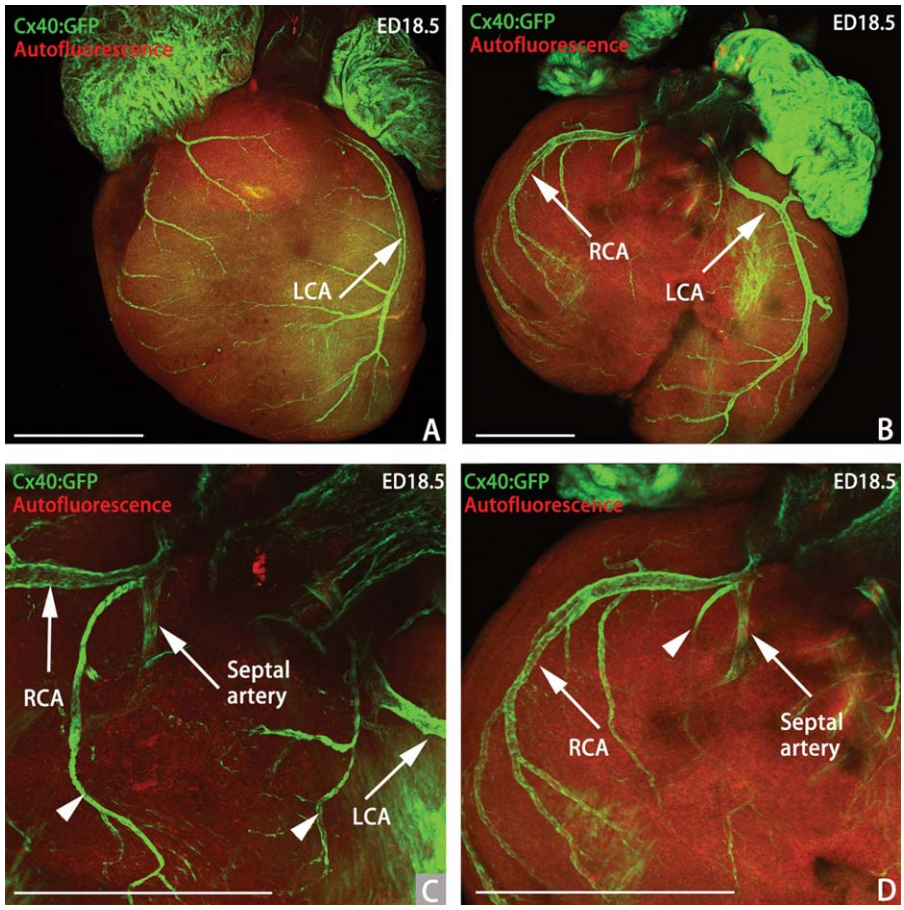

Fig. 2. Coronary arteries at ED18.5 in *Cx40:GFP* transgenic mouse in whole-mount confocal microscopy. Cx40 expression in coronary artery endothelium and in the atria is shown in green and tissue autofluorescence in red. **A,B**: Overview of developed left (LCA) and right (RCA) coronary arteries in the whole heart. Coronary vasculature is already developed up to the apex of the heart. Z-stacks from 20 and 19 sections, respectively, 25 μm per section. **C**: Detailed view of the origin of the LCA, RCA, septal artery, and conus arteries. Z-stack from 17 sections, 12 μm per section. **D**: Magnified view of the RCA with its branches (arrowheads, conus artery and proximal branches of the right ventricle). Z-stack from 16 sections, 15 μm per section. Scale bar = 300 μm.

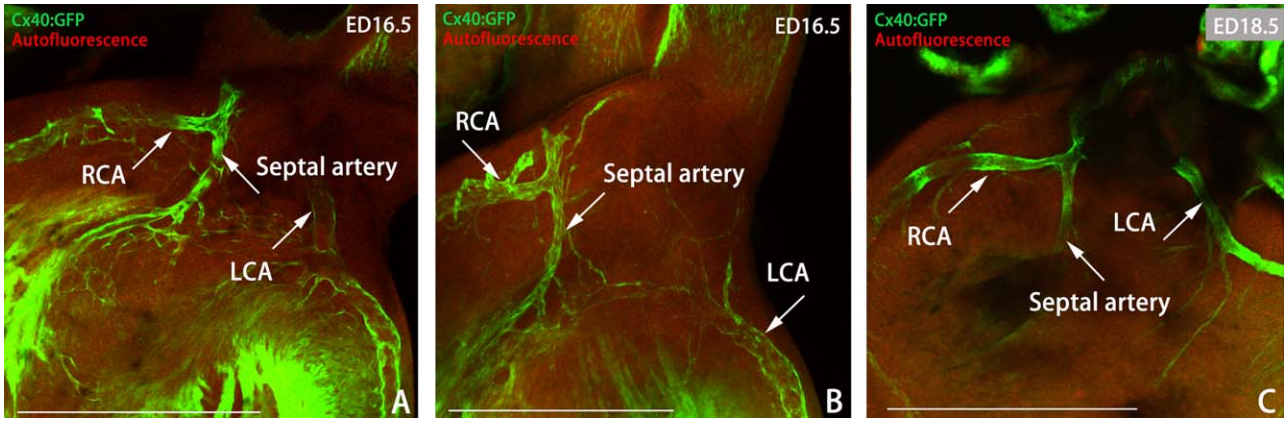

Fig. 3. Formation of the septal artery from a plexus in the embryonic heart in a *Cx40:GFP* transgenic mouse. **A,B**: Stage ED16.5, formation of the septal artery tube from a vascular plexus, connected to the right and left coronary arteries. Z-stacks from 17 and 15 sections, respectively, 25 μm per section. **C**: 18.5ED, the tube of the septal artery is formed, the vascular plexus is remodeled, and the connection to the LCA is lost. Septal artery is a branch of the right coronary artery. Z-stack from 16 sections, 25 μm per section. Scale bars = 300 μm.

Microfil is detectable both visually (due to its yellow color) and with X-rays; therefore, it was possible to analyze the injected hearts on a micro-CT scanner. Micro-CT permitted not only 2D imaging, hence generating sections similar to those obtained with a confocal microscope, but also undistorted 3D images. We were, therefore, able to completely reconstruct the

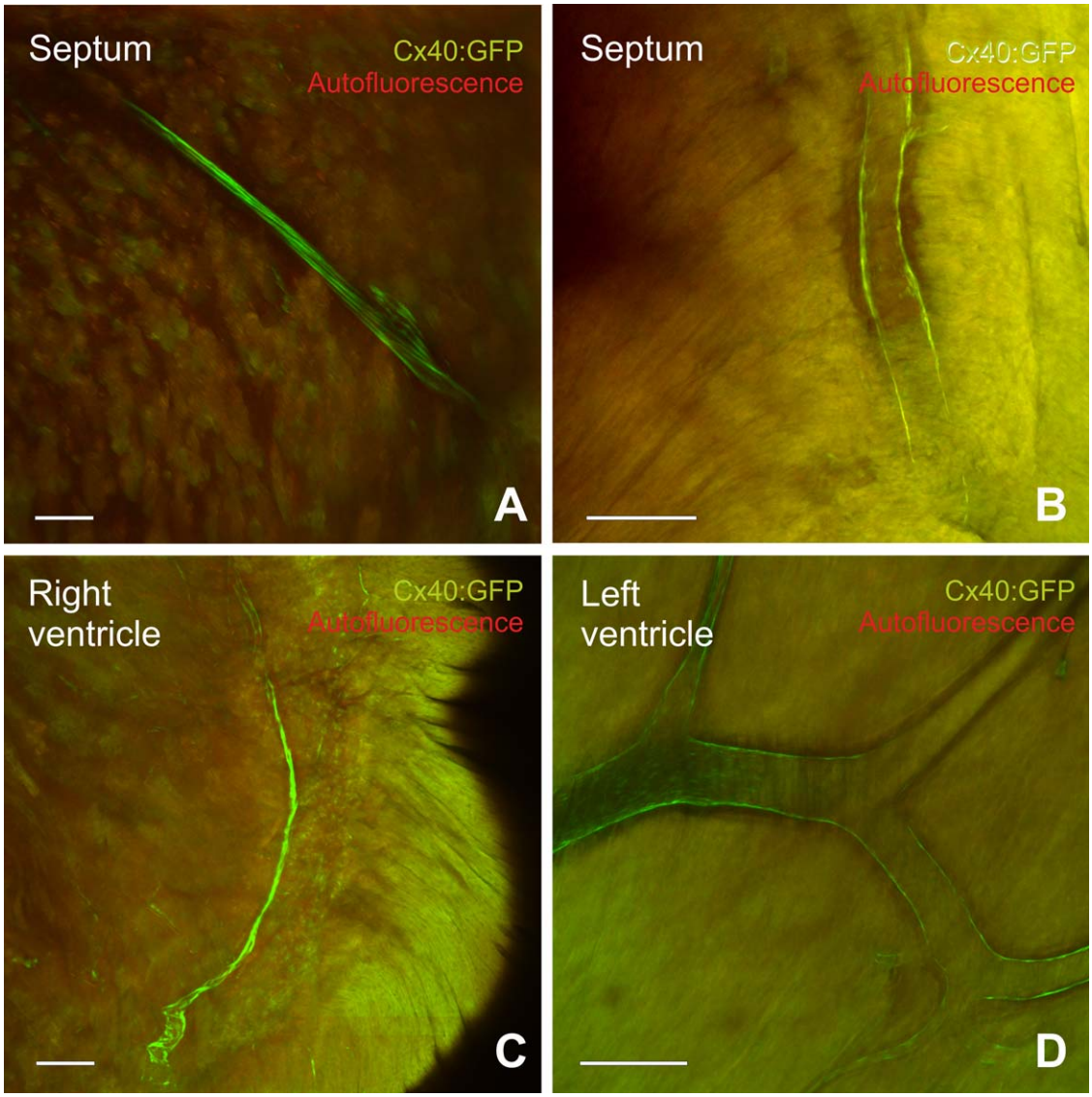

Fig. 4. Coronary arteries in *Cx40:GFP* juvenile transgenic mouse. Visualization of the whole arteries is obscured by the surrounding highly autofluorescent myocardium. **A,B**: Septal artery at lower and higher magnifications, respectively. Z-stack from 5 and 7 sections, 15 μm per section. **C**: Right coronary artery, Z-stack from 8 sections, 15 μm per section. **D**: Left coronary artery. Z-stack from 6 sections, 12 μm per section. Scale bar = 200 μm.

course of the adult mouse coronary vasculature in 3D (Fig. 6, Supp. Video 1).

In juvenile hearts, we were tracking the course of the RCA and LCA with a special focus on the septal artery. The septal artery in juvenile mice started as the first branch of the RCA in all six specimens analyzed. It then continued as a single trunk in the interventricular septum, giving off branches to nourish it, and ended at the apex of the heart. The RCA and LCA coursed through the atrioventricular groove and supplied the right and left ventricles, respectively. The branching pattern was similar to that observed at ED18.5, described earlier in the *Cx40:GFP* knock-in mouse. In the RCA, we were able to distinguish the following branches: *ramus circumflexus dexter, ramus proximalis ventriculi dextri, ramus marginis ventriculi dextri* and *ramus distalis ventriculi dextri*. In the LCA, we observed *ramus circumflexus sinister, ramus interventricularis paraconalis, ramus proximalis ventriculi sinistri, ramus colateralis sinister proximalis, ramus colateralis sinister distalis*, and *ramus ventriculares* (Fig. 7).

Discussion

Here we demonstrate well resolved details of the coronary vasculature in a fluorescent reporter transgenic *Cx40:GFP* mouse model using recently optimized (Kolesová et al., 2016) whole-organ tissue-clearing techniques and confocal microscopy. In addition, we report that the septal artery develops initially from an arterial plexus connected to both coronary arteries but finally remains only as a branch of the RCA in our mouse strain. These data serve as proof of principle of the value of whole-heart clearing coupled with fluorescence reporter systems in high-resolution evaluation of coronary artery development. Given the considerable current interest in coronary artery anatomy and

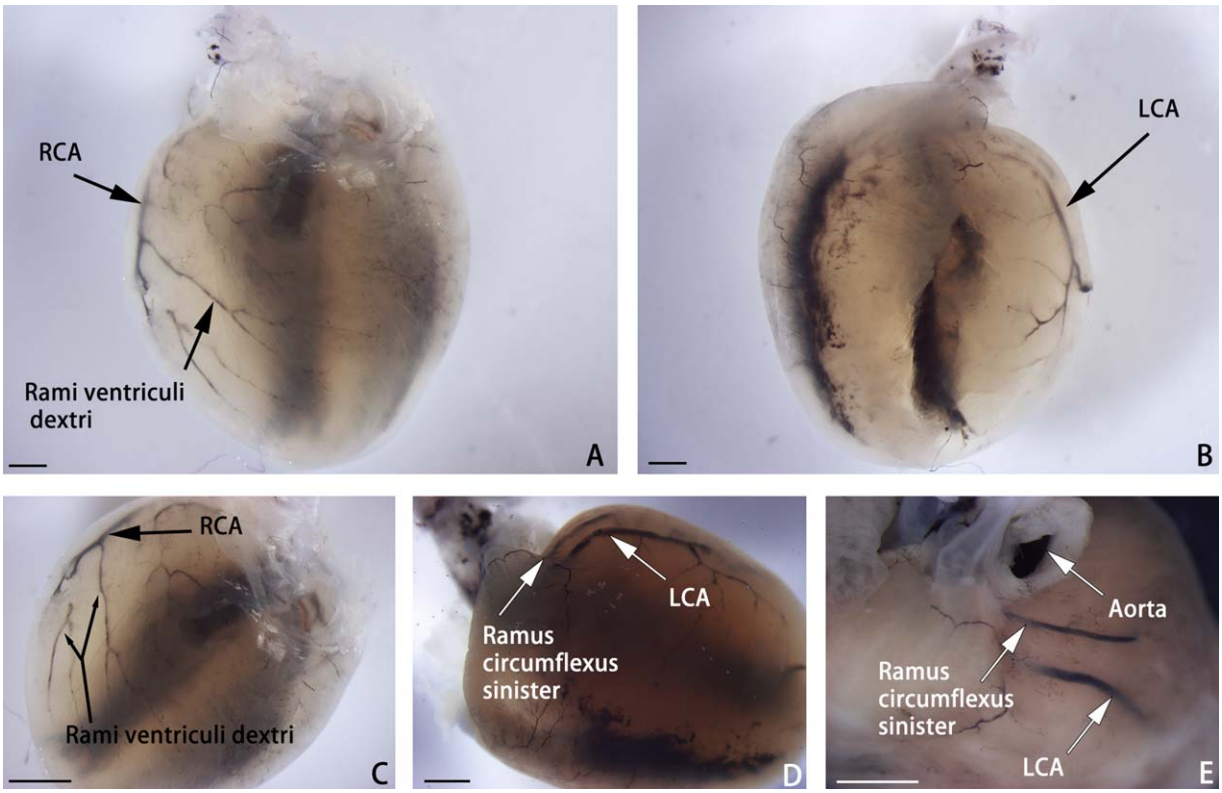

Fig. 5. Coronary vasculature in juvenile mouse hearts visualized with India ink. **A, B**: Overview of the whole heart arteries, especially the right coronary artery (RCA; A) and the left coronary artery (LCA; B) and their branches. **C**: Detailed view of the right coronary artery. **D**: Detailed view of the left coronary artery and the left circumflex artery. **E**: Top and auricular surface. Scale bar = 1 mm.

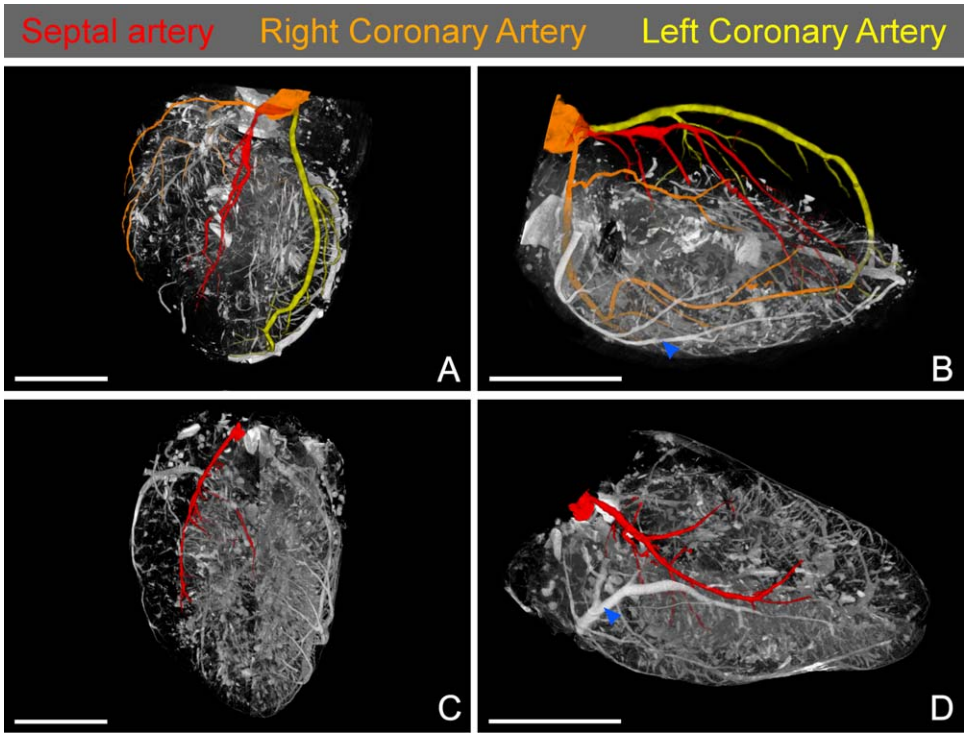

Fig. 6. Coronary vasculature in juvenile mouse hearts visualized with the Microfil injection and micro-CT. Visualization of the right coronary artery (orange), left coronary artery (yellow), and septal artery (red). **A,C**: Anterior aspect; **B,D**: lateral aspect. Arrowheads, *vena cordis dextra*. Scale bar = 2 mm.

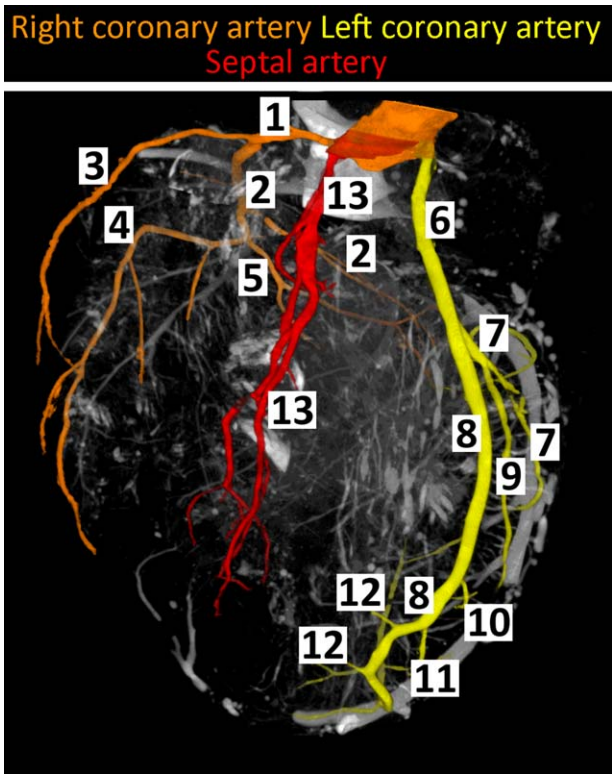

Fig. 7. Overview of the coronary arteries and their branches visualized with Microfil and micro-CT. Right coronary artery (1, orange): 2, *ramus circumflexus dexter;* 3, *ramus proximalis ventriculi dextri;* 4, *ramus marginis ventriculi dextri;* 5, *ramus distalis ventriculi dextri*. Left coronary artery (6, yellow): 7, *ramus circumflexus sinister;* 8, *ramus interventricularis paraconalis;* 9, *ramus proximalis ventriculi sinistri;* 10, *ramus colateralis sinister proximalis;* 11, *ramus colateralis sinister distalis;* 12, *rami ventriculares*. Septal artery (13, red).

development, due to the role of coronary artery anomalies in sudden cardiac death in humans (Spicer et al., 2015) and their remodeling in mouse models of myocardial infarction (Miquerol et al., 2015), the *Cx40:GFP* mouse model could pave the way for detailed—down to a single-cell resolution—analysis of the origin, course, and remodeling of coronary arteries to establish the relationships between anatomy and clinical events.

Recent advances in tissue-clearing techniques and whole-organ imaging have enabled the study of *Cx40:GFP* mice models and GFP expression in whole-mounts. The *Cx40:GFP* mouse models were found to be more suitable for the analysis of expression of Cx40 when compared to immunohistochemistry. The GFP transgene shows cytoplasmic expression and thus labels the entire endothelial cell; this is in contrast to Cx40 antibody staining, which is limited to the cell edges and labels cells in a punctate manner; as a result, it is not considered suitable for 3D reconstructions. Furthermore, whole-mount staining for connexins, while not impossible, is not widely used except on thick sections (Greiner et al., 2018).

Our findings strengthen the role of Connexin40 and its fluorescent reporter model *Cx40:GFP* on the list of possible visualization techniques of coronary arteries, along with PECAM, VE-cadherin, and Tie-2. Kisanuki et al. (2001) have created the Tie2-cre mouse model by expressing the Cre recombinase in the endothelial cell lineage of the heart, but only up to ED11.5, when Tie2 expression was no longer restricted to just the endothelial cells but was found in many other areas of the heart. Combinations of these mice with appropriate reporter strains (LacZ, GFP) also provide the opportunity for genetic labeling of the vasculature. We have used anti-CD31 (PECAM) staining to visualize endothelial/endocardial cells in the hearts of transgenic animals for better characterization of the cardiac phenotype (Vrbacky et al., 2016). While the staining works well in whole-mount up to ED12.5, it was useful only for visualization of the vasculature in the embryo. This method was found to be disadvantageous to study the arterial system in vascularized adult organs that have a rich capillary network.

Recent advances in tissue-clearing techniques permit detailed whole-organ imaging. Although a number of tissue-clearing techniques have been developed for this purpose in recent years (e.g., THF-DBE [Becker et al., 2012], CLARITY [Chung et al., 2013], SCALE [Hama et al., 2011], and CUBIC [Tainaka et al., 2014]), mainly used for whole-brain imaging, not all of them are suitable for cardiovascular developmental studies. As we reported previously (Kolesová et al., 2016), the CUBIC method is most suitable for heart-development imaging, as it sufficiently clears the heart tissues while preserving the GFP signal. For the coronary vasculature study, we also recommended the SCALE clearing technique. SCALE clears only the superficial tissue layers and therefore is not suitable for deeper structures such as trabeculae and the Purkinje network, but it is more than sufficient for mostly superficially located coronary vasculature. SCALE is also cheaper and preserves the fluorescence of tissue samples longer than CUBIC.

The *Cx40:GFP* knock-in mice, where homozygotes are viable and fertile (although with a reduced life span), were previously reported to suffer from hypertension, increased incidence of congenital heart defects, and electrophysiological anomalies. The heterozygotes have GFP positivity in the coronary vasculature, similar to homozygotes, and therefore are completely suitable for coronary artery imaging. From existing literature (Sankova et al., 2012; Benes et al., 2014), it does not appear that heterozygotes harbor any cardiac malformations, including coronary artery defects, which is in concordance with our findings. We found that the branching patterns of the RCA and LCA are in accordance with the previous studies in the Swiss albino mice (Icardo and Colvee, 2001; Yoldas et al., 2010) as well as in the wild-type mice (Durán et al., 1992). These findings confirm that coronary vasculature development and structure are not affected in the *Cx40:GFP* heterozygous mice and can therefore be used as a model for normal coronary artery development.

The *Cx40:GFP* mouse model has its limits in the study of postnatal coronary vasculature, even though GFP positivity in the endothelium of all arteries was still present. Considerable autofluorescence of the surrounding myocardium did not permit any further whole-heart imaging with confocal microscopy. There was, however, no problem in distinguishing the coronary endothelium from the (also GFP-positive) Purkinje network, as the two systems clearly differed in their anatomical location (superficial vs. subendocardial) and morphology (hollow tubular network vs. solid web). Therefore, we recommend India ink injection for examinations of the juvenile and adult hearts due to its easy application and fast analysis of the gross anatomy in coronary vasculature (Nanka et al., 2008). For a more detailed analysis of the adult arterial and venous network, we propose the Microfil injection method followed by analysis of the specimen with micro-CT (Zagorchev et al., 2010; Sangaralingham et al., 2012),

which permits analysis of the whole 3D structure of the vasculature (Ghanavati et al., 2014). Unlike corrosion casting (Kolesová et al., 2007), the Microfil injection/micro-CT analysis includes the surrounding soft tissues, thus better preserving the spatial relationships on the specimen (Clauss et al., 2006). An additional advantage of using this contrast medium lies in the option of specimen analysis by a micro-CT scanner that enabled increased 3D spatial resolution and imaging (Butcher et al., 2007); this is in contrast to other vascular casting methods, i.e. corrosion cast with Mercox and scanning electron microscopy analysis, which only produced 2D images without complete spatial information (Kolesová et al., 2007).

Regarding the example of septal artery development, we demonstrate the possibility of using the *Cx40:GFP* mouse model for the study of development and remodeling of the arterial plexuses. For the first time here, we highlight information regarding the development of the septal artery from an arterial plexus, followed by its remodeling into a single tube connected to the RCA, as observed in all the embryos that were analyzed. The development of the septal artery in late fetal stages explains the variability among different mouse strains. The connection of the septal artery is established just two days before birth, where it was initially connected to both coronary stems by an arterial plexus. However, subtle differences in plexus remodeling can result in connections of the septal artery to the RCA or LCA, or in it arising separately from the aorta as development progresses. Remodeling of this plexus can account for the variability found previously (López-García et al., 2016) in frequently used laboratory mouse strains: The septal artery arose from the RCA in 32% (C57BL/6), 78% (Balb/c), 67% (CD2F1), 80% (129sv x BL/6), and 87% (wild mouse) of cases. The low proportion of septal arteries arising from the RCA in C57BL/6 mice mirrors an earlier report of frequently abnormal coronary arteries in this strain, including solitary ostia, accessory ostia, high takeoff, aortic intramural course, slit-like ostia, lock-like ostia, and low proportion of septal arteries arising from the RCA (35%) (Fernandez et al., 2008). Furthermore, two septal arteries, each with different origins, may coexist (Salto-Tellez et al., 2004; Fernandez et al., 2008). In the iv/iv mice, coronary artery abnormalities such as high takeoff, double origins, a single coronary orifice, and slit-like openings were found in 84% of mice (Icardo and Colvee, 2001); these were similar to some coronary anomalies described in humans. Crossing of these lines on the *Cx40:GFP* background would provide further understanding of coronary artery development and malformations.

Coronary anomalies are significant since they occur sporadically in man and are found in approximately 0.2%–1% of coronary angiograms and 0.3% of autopsies (Tuncer et al., 2006; Gul et al., 2014). The majority of coronary artery anomalies are benign variations located at the origin of the coronary artery and are asymptomatic (Gul et al., 2014). However, some coronary artery anomalies are known to contribute to cardiovascular mortality and morbidity, so understanding of coronary vasculature development from mouse models can also improve our understanding of human coronary abnormalities. The combined methods presented here are likely to be useful in finding laboratory correlates of human coronary artery abnormalities that result in sudden cardiac death. Detailed characterization of coronary artery anatomy in mice will enable selection of the most appropriate strain for future translational studies.

Experimental Procedures

Animals

The *Cx40:GFP* knock-in mice (Miquerol et al., 2004) were maintained in a homozygous state (as these animals are viable and fertile) and crossed with the wild-type Swiss albino mouse strain to produce heterozygous embryos without heart malformations (Simon et al., 1998). Male and female animals were caged together overnight; ED0.5 was considered midday of the day the vaginal plug was detected. Pregnant females were sacrificed by cervical dislocation on ED16.5 (n = 13 embryos) and ED18.5 (n = 10 embryos). The fetuses were rapidly dissected out of the membranes and perfusion-fixed with freshly prepared 4% (wt/vol) paraformaldehyde, followed by immersion in the same fixative for 48 hr. Juvenile mice at 14 and 30 days were also sacrificed by cervical dislocation followed by rapid chest opening and perfusion fixation of the hearts with 4% (wt/vol) paraformaldehyde in a manner similar to that used for the embryos (n = 3 per stage). Embryos or isolated hearts were then rinsed with phosphate buffered saline (PBS) and treated with SCALE or CUBIC tissue-clearing protocols (see below) in Tissue Clearing. All applicable international, national, and institutional guidelines for the care and use of animals were followed. All tissues were isolated in accordance with the ethical standards of the Charles University, with protocols approved by the Animal Care and Use Committee of the First Faculty of Medicine.

Tissue Clearing: CUBIC, SCALE

Embryonic and adult *Cx40:GFP* knock-in mice were analyzed in the whole-mount using tissue-clearing methods. The CUBIC protocol (clear, unobstructed brain-imaging cocktail) was originally described for brain specimens (Susaki et al., 2014). Briefly, CUBIC solution (N,N,N,N-tetrakis(2-hydroxypropyl) ethylenediamine 25% (wt/vol), urea 25% (wt/vol), and polyethylene glycol monopisooctylphenyl ether (Triton X-100) 15% (wt/vol in water) was thoroughly mixed for 30 min at 37 °C and then kept at room temperature. All specimens were submerged and gently rocked in the CUBIC solution at 37 °C. Specimens were placed in fresh CUBIC solution every 3–4 days. All chemicals were obtained from Sigma-Aldrich (Darmstadt, Germany) except for Triton-X (Roth, Karlsruhe, Germany).

As demonstrated in previous studies (Kolesová et al., 2016), CUBIC solution is ideal for simultaneously clearing the embryonic heart tissue and preserving the GFP signal. Alternatively, a SCALE clearing protocol (Hama et al., 2011) was used, since the coronary vascular study required only clearing of the superficial layers of the heart.

Confocal Microscopy Imaging

High-resolution images were obtained with a single-photon confocal system FluoView FV1000 fitted on an upright BX61 microscope (Olympus, Tokyo, Japan), using 4x (NA 0.16, WD 13mm) and 10x (NA 0.40, WD 3.1mm) dry objective. The appropriate filter sets were used in order to properly capture GFP (488 nm excitation) and autofluorescence (543 nm). Whole embryos were imaged in custom-made chambers (Miller et al., 2005) immersed in CUBIC solution and covered with a coverslip. All images were assembled and analyzed in ImageJ (NIH, Bethesda, MD) and merged using Photoshop (Adobe Systems, San Jose, CA).

India ink Injection

Adult hearts were injected retrogradely via the aorta with a solution of India ink diluted in PBS (1:5) (Nanka et al., 2008). Following the injection, the hearts were fixed for at least 24 hr in 4% paraformaldehyde. After clearing the specimens in SCALE, coronary vasculature of each heart was studied under a dissecting microscope. The hearts were then photographed under the dissecting microscope (Olympus, Tokyo, Japan) in a glass Petri dish, without a coverslip, in SCALE using an Olympus DP50 CCD camera.

Microfil Injection

Juvenile mice (30 day old, n = 6) were sacrificed by cervical dislocation and the hearts were rapidly excised and retrogradely perfused under a constant flow of 2.5 ml/min with non-recirculating Tyrode's buffer (mmol/l: NaCl 145, KCl 5.9, CaCl2 1.1, MgCl2 1.2, glucose 11, HEPES 5; pH 7.4), gassed with 100% O_2, and maintained at 37 °C. After 5 min of stabilization, the hearts were perfused for another 5 min by Tyrode's buffer with 5 mM adenosine (Sigma-Aldrich, Czech Republic) to induce vasodilatation, followed by 2 min of perfusion with a cardioplegic solution (NaCl 110.0 mM, NaHCO3 10.0 mM, KCl 16.0 mM, MgCl2 16.0 mM, CaCl2 1.2 mM, pH 7.8). After that, the Microfil (1–1.5 ml; Flow Tech, Carver, MA) was retrogradely administrated into the coronary bed by slow infusion. The whole injecting procedure was performed according to the Microfil producer's recommendations and the protocol by Weyers and colleagues (Weyers et al., 2012). The hearts were stored for 2 hr at -20 °C to allow polymerization of Microfil and then fixed in 4% paraformaldehyde for 48 hr at 4 °C. After fixation and thorough rinsing with PBS, the hearts were processed by micro-CT.

Micro-CT Imaging

Mouse hearts (n = 6) X-ray contrasted with Microfil injection were scanned using a desktop ex vivo micro-CT device SkyScan 1272 (Bruker, Bruxelles, Belgium). Each specimen was placed in a plastic tube with PBS and mounted on a microstage, and underwent micro-CT scanning according to the following parameters: pixel size 4 μm, source voltage 60 kV, source current 166 μA, rotation step 0.1°, Al filter 0.25 mm, frame averaging 3, rotation 180°. The scanning time was approximately 4 hr for each specimen.

Data sets of projection images were reconstructed into cross-section images using NRecon software (Bruker). The effect of computed tomography artifacts (e.g., misalignment, ring artifacts, and beam hardening) was reduced by NRecon software corrections. 3D visualizations were rendered using CTVox (Bruker).

After identification of the septal artery in 3D visualization, the image analysis software CTAn (Bruker) was employed. A region of interest (ROI) comprising the septal artery was set by hand-drawn selection in the data set of cross-section images. This allowed the creation of a volume of interest (VOI) that included only the septal artery. The ROI selection was complicated, in some areas, by void spaces created by improper contrast filling; this was often seen in the branching areas. If the artery behind this gap was considered a possible branch of the septal artery, it was included in the ROI selection. In the same manner, the RCA and LCA were defined. Visualization of the original dataset was combined with RCA, LCA, and septal artery data sets, which enabled 3D visualization of the whole specimen using CTVox. Selected arteries were depicted in color, while the original data set was kept in grayscale to improve image clarity.

Acknowledgments

We would like to express our thanks to Ms. Marie Jindraková for her excellent technical assistance, and Ms. Shreiya Narayanan for language editing. The micro-CT part of the study is a result of implementation of the project "Technological development of post-doc programs," registration number CZ.1.05/41.00/16.0346, supported by Research and Development for Innovations Operational Programme (RDIOP), and co-financed by the European regional development fund and the state budget of the Czech Republic.

References

Andersen TA, Troelsen Kde L, Larsen LA. 2014. Of mice and men: molecular genetics of congenital heart disease. Cell Mol Life Sci 71:1327–1352.

Becker K, Jahrling N, Saghafi S, Weiler R, Dodt HU. 2012. Chemical Clearing and Dehydration of GFP Expressing Mouse Brains. PLoS One 7:e33916.

Benes J Jr, Ammirabile G, Sankova B, Campione M, Krejci E, Kvasilova A, Sedmera D. 2014. The role of connexin40 in developing atrial conduction. FEBS Lett 588:1465–1469.

Butcher JT, Sedmera D, Guldberg RE, Markwald RR. 2007. Quantitative volumetric analysis of cardiac morphogenesis assessed through micro-computed tomography. Dev Dyn 236(3):802–809.

Chung K, Wallace J, Kim SY, Kalyanasundaram S, Andalman AS, Davidson TJ, Mirzabekov JJ, Zalocusky KA, Mattis J, Denisin AK, Pak S, Bernstein H, Ramakrishnan C, Grosenick L, Gradinaru V, Deisseroth K. 2013. Structural and molecular interrogation of intact biological systems. Nature 497:332–337.

Clauss SB, Walker DL, Kirby ML, Schimel D, Lo CW. 2006. Patterning of coronary arteries in wildtype and connexin43 knockout mice. Dev Dyn 235:2786–2794.

Durán AC, Sans-Coma V, Arque JM, Cardo M, Franco D. 1992. Blood Supply to the Interventricular Septum of the Heart in Rodents with Intramyocardial Coronary Arteries. Acta Zoologica 73:223–229.

Fernandez B, Durán AC, Fernandez MC, Fernandez-Gallego T, Icardo JM, Sans-Coma V. 2008. The coronary arteries of the C57BL/6 mouse strains: implications for comparison with mutant models. J Anat 212:12–18.

Ghanavati S, Yu LX, Lerch JP, Sled JG. 2014. A perfusion procedure for imaging of the mouse cerebral vasculature by X-ray micro-CT. J Neurosci Methods 221:70–77.

Greiner J, Sankarankutty AC, Seemann G, Seidel T, Sachse FB. 2018. Confocal Microscopy-Based Estimation of Parameters for Computational Modeling of Electrical Conduction in the Normal and Infarcted Heart. Front Physiol 9:239.

Gul M, Sen F, Sahan E, Maden O, Selcuk T. 2014. Right coronary artery emerging as a septal branch from the left anterior descending artery: a single coronary ostium anomaly. Herz 39: 780–782.

Hama H, Kurokawa H, Kawano H, Ando R, Shimogori T, Noda H, Fukami K, Sakaue-Sawano A, Miyawaki A. 2011. Scale: a chemical approach for fluorescence imaging and reconstruction of transparent mouse brain. Nat Neurosci 14:1481–1488.

Icardo JM, Colvee E. 2001. Origin and course of the coronary arteries in normal mice and in iv/iv mice. J Anat 199:473–482.

Kisanuki YY, Hammer RE, Miyazaki J, Williams SC, Richardson JA, Yanagisawa M. 2001. Tie2-Cre transgenic mice: a new model for endothelial cell-lineage analysis in vivo. Dev Biol 230:230–242.

Kolesová H, Capek M, Radochova B, Janacek J, Sedmera D. 2016. Comparison of different tissue clearing methods and 3D imaging techniques for visualization of GFP-expressing mouse embryos and embryonic hearts. Histochem Cell Biol 146:141–152.

Kolesová H, Lametschwandtner A, Rocek Z. 2007. The evolution of amphibian metamorphosis: insights based on the transformation of the aortic arches of Pelobates fuscus (Anura). J Anat 210: 379–393.
Leaf DE, Feig JE, Vasquez C, Riva PL, Yu C, Lader JM, Kontogeorgis A, Baron EL, Peters NS, Fisher EA, Gutstein DE, Morley GE. 2008. Connexin40 imparts conduction heterogeneity to atrial tissue. Circ Res 103:1001–1008.
Lee YT, Lin HY, Chan YW, Li KH, To OT, Yan BP, Liu T, Li G, Wong WT, Keung W, Tse G. 2017. Mouse models of atherosclerosis: a historical perspective and recent advances. Lipids Health Dis 16: 12.
López-García A, Soto-Navarrete MT, Fernandez MC, Moncayo-Arlandi J, Durán AC, López-Unzu MA, Alonso-Briales JH, Fernandez B. 2016. Unusual anatomical origins of the coronary arteries in C57BL/6 mice. Are they strain-specific? J Anat 229: 703–709.
Michael LH, Entman ML, Hartley CJ, Youker KA, Zhu J, Hall SR, Hawkins HK, Berens K, Ballantyne CM. 1995. Myocardial ischemia and reperfusion: a murine model. Am J Physiol 269:H2147–2154.
Miller CE, Thompson RP, Bigelow MR, Gittinger G, Trusk TC, Sedmera D. 2005. Confocal imaging of the embryonic heart: How deep? Microscop Microanal 11:216–223.
Miquerol L, Meysen S, Mangoni M, Bois P, van Rijen HV, Abran P, Jongsma H, Nargeot J, Gros D. 2004. Architectural and functional asymmetry of the His-Purkinje system of the murine heart. Cardiovasc Res 63:77–86.
Miquerol L, Thireau J, Bideaux P, Sturny R, Richard S, Kelly RG. 2015. Endothelial plasticity drives arterial remodeling within the endocardium after myocardial infarction. Circ Res 116:1765–1771.
Nanka O, Krizova P, Fikrle M, Tuma M, Blaha M, Grim M, Sedmera D. 2008. Abnormal myocardial and coronary vasculature development in experimental hypoxia. Anat Rec (Hoboken) 291:1187–1199.
Salto-Tellez M, Yung Lim S, El-Oakley RM, Tang TP, ZA AL, Lim SK. 2004. Myocardial infarction in the C57BL/6J mouse: a quantifiable and highly reproducible experimental model. Cardiovasc Pathol 13:91–97.
Sangaralingham SJ, Ritman EL, McKie PM, Ichiki T, Lerman A, Scott CG, Martin FL, Harders GE, Bellavia D, Burnett JC Jr. 2012. Cardiac micro-computed tomography imaging of the aging coronary vasculature. Circ Cardiovasc Imaging 5:518–524.
Sankova B, Benes J Jr, Krejci E, Dupays L, Theveniau-Ruissy M, Miquerol L, Sedmera D. 2012. The effect of connexin40 deficiency on ventricular conduction system function during development. Cardiovasc Res 95:469–479.
Simon AM, Goodenough DA, Paul DL. 1998. Mice lacking connexin40 have cardiac conduction abnormalities characteristic of atrioventricular block and bundle branch block. Curr Biol 8:295–298.
Spicer DE, Henderson DJ, Chaudhry B, Mohun TJ, Anderson RH. 2015. The anatomy and development of normal and abnormal coronary arteries. Cardiol Young 25:1493–1503.
Susaki EA, Tainaka K, Perrin D, Kishino F, Tawara T, Watanabe TM, Yokoyama C, Onoe H, Eguchi M, Yamaguchi S, Abe T, Kiyonari H, Shimizu Y, Miyawaki A, Yokota H, Ueda HR. 2014. Whole-brain imaging with single-cell resolution using chemical cocktails and computational analysis. Cell 157:726–739.
Tainaka K, Kubota SI, Suyama TQ, Susaki EA, Perrin D, Ukai-Tadenuma M, Ukai H, Ueda HR. 2014. Whole-body imaging with single-cell resolution by tissue decolorization. Cell 159:911–924.
Tuncer C, Batyraliev T, Yilmaz R, Gokce M, Eryonucu B, Koroglu S. 2006. Origin and distribution anomalies of the left anterior descending artery in 70,850 adult patients: multicenter data collection. Catheter Cardiovasc Interv 68:574–585.
van Rijen HV, van Veen TA, van Kempen MJ, Wilms-Schopman FJ, Potse M, Krueger O, Willecke K, Opthof T, Jongsma HJ, de Bakker JM. 2001. Impaired conduction in the bundle branches of mouse hearts lacking the gap junction protein connexin40. Circulation 103:1591–1598.
Vrbacký M, Kovalčková J, Chawengsaksophak K, Beck IM, Mráček T, Nůsková H, Sedmera D, Papoušek F, Kolář F, Sobol M, Hozák P, Sedlacek R, Houštěk J. 2016 Knockout of Tmem70 alters biogenesis of ATP synthase and leads to embryonal lethality in mice. Hum Mol Genet 1;25(21):4674–4685.
Wagner C, de Wit C, Kurtz L, Grunberger C, Kurtz A, Schweda F. 2007. Connexin40 is essential for the pressure control of renin synthesis and secretion. Circ Res 100:556–563.
Weyers JJ, Carlson DD, Murry CE, Schwartz SM, Mahoney WM Jr. 2012. Retrograde perfusion and filling of mouse coronary vasculature as preparation for micro computed tomography imaging. J Vis Exp:e3740.
Yoldas A, Ozmen E, Ozdemir V. 2010. Macroscopic description of the coronary arteries in Swiss albino mice (Mus musculus). J S Afr Vet Assoc 81:247–252.
Zagorchev L, Oses P, Zhuang ZW, Moodie K, Mulligan-Kehoe MJ, Simons M, Couffinhal T. 2010. Micro computed tomography for vascular exploration. J Angiogenes Res 2:7.